Understanding Bending Losses in Holey Optical Fibers

Joanne C. Baggett * Tanya M. Monro, Kentaro Furusawa, Vittoria Finazzi, D. J. Richardson

Optoelectronics Research Centre, University of Southampton, Southampton SO17 1BJ, UK

Abstract

Extremely large mode area fibers that are single-moded over a broad wavelength range can be created using holey fiber technology. However, as with any fiber, the largest mode areas that are practically feasible are ultimately determined by bending losses. It is therefore essential to gain an understanding of the factors that influence bend loss in these fibers in order to form accurate predictions that can facilitate improved bend loss design. Here we present the first detailed study of transition loss and pure bend loss in a holey fiber and consider the impact of the fiber structure. A theoretical model is derived that retains the full refractive index profile of a holey fiber. This approach is used to predict the bend loss in large mode area holey fibers and is validated through comparison with experimental data. For the fibers under study here, we demonstrate that pure bend loss is the dominant component of macro-bend loss and that the hole configuration within the cladding can strongly influence this loss.

Key words: Holey fibers, Microstructured fibers, Photonic crystal fibers, Bend loss, Curvature loss, Pure bend loss, Transition loss

1 Introduction

1.1 Large mode area holey fibers

Large mode area optical fibers are required in high power applications, including laser welding and machining and active devices such as fiber lasers and amplifiers. For many of these applications, single-moded operation is also an essential requirement. In conventional solid optical fibers, enlarging the core and decreasing the numerical aperture (NA) both act to increase the fundamental mode area. The challenge of accurately controlling low dopant concentrations places an upper limit on the smallest NA (and hence the largest mode area) that can be achieved using conventional technology. Despite this, single-mode fibers with mode areas as large as $400\mu m^2$ at 1550nm have been achieved [1]. Since the NA must also reduce with wavelength in order to maintain single-moded guidance, these fabrication challenges become more pronounced for fibers designed for use at short wavelengths.

Holey fiber (HF) technology has emerged as an alternative route towards large mode areas [2]. The guidance mechanism in a HF results from the effective index difference between the solid core and the microstructured cladding, which is defined by an array of air holes. Large mode areas can be engineered by increasing the hole-to-hole spacing (Λ), by decreasing the hole diameter (d),

* Corresponding author
Email address: jcb@orc.soton.ac.uk (Joanne C. Baggett).

or both. Increasing Λ is analogous to enlarging the core size in a conventional fiber, while decreasing d allows the field to penetrate further into the cladding and is equivalent to reducing the NA in a conventional fiber.

HFs are typically fabricated from glass tubes that are stacked around a solid silica rod and are drawn to fiber using a conventional fiber drawing tower [3]. This fabrication process enables the creation of a diverse range of fibers with a wide range of optical properties, including *endlessly* single-moded guidance [4]. This unique optical property means that a single silica fiber can offer broad-band single-mode operation extending from the ultra-violet to the infra-red. Given that one fiber can be used for all wavelengths, there are no additional fabrication difficulties associated with short wavelength operation, which is an advantage over conventional techniques. In addition, since it is possible to fabricate HFs with air holes as small as 50nm in diameter, such fibers can offer extremely low numerical apertures.

Although HF technology may offer advantages over conventional techniques, the largest mode sizes that can be tolerated in practice are, as in any fiber, determined by the bending losses. Moreover, for practical devices, compact packaging is desirable. It is therefore essential to gain an understanding of the factors that influence bend loss in HFs in order to accurately predict these losses.

1.2 Bending losses in holey fibers

Bend loss is traditionally separated for convenience into two regimes; *macro-bending* and *micro-bending* losses [5]. Macro-bending losses result from bends

that are significantly greater in scale than the fiber core, while micro-bending losses occur for small-scale bends, along which the mode distorts continuously. Micro-bends generally result from waveguide coating, cabling, packaging and installation and can be reduced through careful processing and handling. In this study we concentrate on the macro-bend loss regime. Our aim is to determine the largest mode areas that can be tolerated in practical applications.

As light encounters a macro-bend in an optical fiber, the modal field distorts radially outwards in the direction of the bend, inducing coupling from the core mode(s) to radiation modes and also to leaky higher order, cladding and backward propagating modes. In conventional fibers, this loss is often separated into two components; *transition loss* and *pure bend loss* [6]. Transition loss, which is also referred to as mode-conversion loss, is a one-off loss that results from the modal distortion induced by the abrupt change in curvature at the beginning and end of a bend. Pure bend loss is defined as the continual loss of radiation from the distorted mode that occurs along any curved section of fiber. Although this distinction between transition and pure bend loss may seem somewhat artificial at first sight, this approach is frequently, and successfully, employed in studies of both slab waveguides and optical fibers [7–15]. Indeed, by considering different types of bend, we can see that these components represent relevant physical quantities. For example, bend loss in long lengths of spooled fiber will be dominated by pure bend loss, while in lengths of fiber with many separate macro-bends, the multiple transition regions can contribute significantly to the overall bend loss.

The bending losses of HFs differ qualitatively from those of conventional step index fibers. Like conventional fibers, HFs exhibit a bend loss edge at long wavelengths due to the fact that the mode extends further into the cladding,

resulting in a more weakly guided mode that will suffer a greater perturbation in response to bending. HFs also possess an additional bend loss edge at short wavelengths as a direct consequence of their novel cladding structure [4]. This can be understood as follows; in a HF the NA decreases towards short wavelengths due to the fact that the mode is more tightly confined to the core and samples less of the air holes. This property gives rise to broadband single-moded guidance, mentioned previously, and also leads to weak guidance and hence less resistance to bending towards shorter wavelengths. This loss edge can also be characterized by the hole-to-hole spacing, Λ; if Λ is large compared with the wavelength, when the fiber is bent, the guided mode can escape via the solid silica bridges between neighboring holes. It has been shown empirically that the optimal bend loss between the two loss edges is approximately given by $\Lambda/2$ [16]. This implies that for the large mode fibers in this study, which have Λ in the range 7.6 - 11.3 μm, standard telecommunications wavelengths lie on the short wavelength side of the optimal point of $\Lambda/2$. At first sight, this may seem to suggest that the bend loss for HFs will be worse than for their conventional counterparts as the bending losses of conventional fibers do not increase towards short wavelengths. However, we have previously demonstrated [1] that the losses at 1550nm are comparable. Moreover, whilst a HF can guide a single mode over a broad wavelength range, the number of modes guided by a conventional step index fiber increases towards short wavelengths. It would therefore be necessary to consider a different conventional fiber at each wavelength in order to make a meaningful comparison between the bending losses of the two fiber types.

An important difference between conventional and holey fibers is the complex nature of the transverse refractive index profile. Unlike conventional fibers,

HFs usually possess a six fold symmetry, which may be reflected in the bending losses. In this paper we present results from a detailed study into the bend loss characteristics of HFs. To assess the potential benefits offered by HFs it is necessary to fully understand how the structure of the fiber can influence these losses. We also consider for the first time the relative contributions from the two components of macro-bend loss; transition loss and pure bend loss.

1.3 The fibers

In this study, four large mode holey fibers (HF1-HF4) and one conventional fiber (C1) were characterized in terms of bend loss. All of the HFs used in this study were drawn from the same preform and the smallest fiber, HF1, is shown in Fig. 1. In each of these fibers, which are made entirely from pure silica, the core is offset from the center of the fiber by one period. This offset was introduced because the same cladding configuration was used to make a cladding pumped HF laser, in which the offset is used to enhance the modal overlap between the core and cladding modes [17].

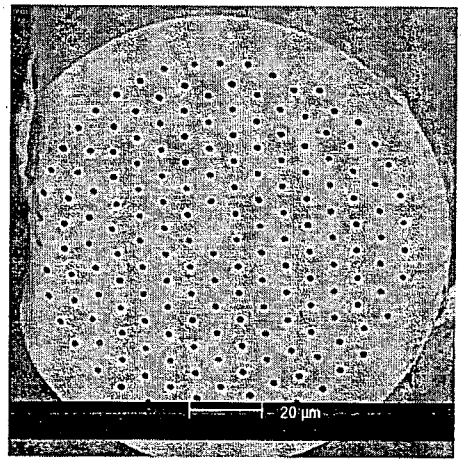

Fig. 1. Holey fiber HF1: hole-to-hole spacing (Λ) = 7.55 μm, hole diameter (d) = 1.71 μm.

For each fiber, the mode field diameter (MFD) was extracted by performing divergence measurements using a standard scanning knife-edge technique [18]. In this approach, we assume a Gaussian transverse field profile and thus define the MFD as twice the distance over which the intensity drops to $1/e^2$ of its maximum value. Although the modes of the HFs we consider here are slightly hexagonal in shape, we observe that the transverse field profiles can be well approximated by a Gaussian function for any given angular orientation. Using this technique, we thus extract a range of MFD values depending on the angular orientation of the fiber. (For any given angular orientation, we estimate that the error in the MFD measurement resulting from imperfect cleaves and alignment is approximately 5%.) The effective area is assumed to be $A_{eff} = (\pi\,MFD^2)/4$, as for a Gaussian mode profile. By averaging the measured MFD values over the different orientations, a representative value for the MFD and hence A_{eff} can be found.

As described in Section 2.2, we can predict the modal properties of these fibers using the full refractive index profile. Our theoretical predictions show that, for the type of fiber considered here, the variation in mode width with angular orientation is approximately 15%. As mentioned above, we extract a representative value of A_{eff} by averaging over MFD measurements for different angular orientations of the fiber. In this way we measure effective areas that agree to within 10% of our predicted values.

The measured effective mode areas, extracted from the divergence measurements, are listed in Table 1 for each fiber included in this study. The effective mode areas range from $130\mu m^2$ to $230\mu m^2$ at 1550nm. For comparison, conventional SMF28 telecommunications fiber has a mode area of approximately $85\mu m^2$ at 1550nm [19], and the largest mode area (of a single-mode fiber)

achieved with conventional technology is around $400\mu m^2$ at 1550nm [1]. Although endlessly single-mode HFs have been demonstrated with effective areas as large as $680\mu m^2$ at 1550nm [1], here we choose to study HFs with more conservative mode areas, which possess reasonably low bending losses. However, in future this work could be extended to larger mode area HFs.

Table 1

Fundamental mode area (A_{eff}) for holey fibers HF1-4 and the conventional step-index fiber C1. The HF parameters are extracted from scanning electron microscope images.

Fiber	**NA**	**a[μm]**	**A_{eff}[μm^2] @ 1.55 μm**	
C1	0.11	4.0	126	
Fiber	**Λ[μm]**	d/Λ	**A_{eff}[μm^2]**	
			@ 1.55 μm	**@ 633 nm**
HF1	7.6	0.23	130	72
HF2	9.7	0.23	215	100
HF3	11.3	0.24	230	103
HF4	9.5	0.25	180	98

1.4 Outline

In the following sections we derive theoretical models to predict the bending losses in HFs and describe the experimental techniques used to investigate the factors that influence these losses. These techniques are used here to study the following aspects of bend loss in HFs; bend loss as a function of radius of

curvature, the components of bend loss and the effect of the fiber geometry on bend loss.

2 Modeling the bending losses of holey fibers

2.1 Background

Predicting the bending losses of HFs is a challenging problem. Most of the methods developed for conventional fibers assume a circularly symmetric index profile and cannot be applied to HFs without first replacing the complex refractive index profile with that of an equivalent step index (ESI) fiber. This approach has been used in a few studies on the modal properties of HFs with mixed results. In Ref. [4], the authors demonstrate that the position of the short wavelength loss edge for a fiber with $\Lambda = 2.3\mu$m and $d = 0.35\mu$m can be qualitatively described by an approximate model of pure bend loss, derived for step index fibers, if the holey fiber is first approximated by an ESI fiber. In another study, an ESI-based calculation of pure bend loss yields good agreement with experimental data for a fiber with $\Lambda = 7.8\mu$m and $d = 2.4\mu$m, but not for a fiber with $\Lambda = 10\mu$m and $d = 5.5\mu$m [16,20]. This poor agreement is due in part to the difficulties in choosing certain ESI parameters, such as core radius, that are required to assign an appropriate ESI profile [21].

In order to avoid this problem we choose to retain the full transverse refractive index profile, and hence the exact mode shape in our calculations of bend loss. As a result, we are also able to study the effects of the angular orientation of the fiber in the bend. We believe this is necessary in order to accurately understand the bending losses of these fibers. This is supported by our ex-

perimental observations of bend loss, in which a dependence on the angular orientation of the fiber has been observed (see Section 3).

For practical fiber devices, we require bends as small as 5-10 centimeters in radius, which are in the macro-bend regime for the fibers considered here. In studies of macro-bending losses in conventional single-mode fibers, pure bend loss is generally assumed to be dominant and transition loss is only considered to be an important contribution for very short lengths of curved fiber [9,22]. Indeed, the effect of mode distortion is often ignored completely in the macro-bend regime [23,24]. However, as very little is known about the relative contributions of the two components of loss in HFs, we consider both pure bend loss and transition loss experimentally and theoretically. The approaches used here to calculate these losses are adapted from techniques that have been developed for conventional waveguides and require both the modal field of the straight fiber and the distorted modal field of the bent fiber.

There are many well documented techniques that can be used to investigate the modal properties of bent step-index fibers. The vast majority of these use a conformal transformation to replace the bent fiber with a straight fiber that has an equivalent refractive index profile. The conformal transformation creates an equivalent fiber by superimposing a gradient onto the refractive index profile of the straight fiber, as described in Section 2.3. The transformed structure (an example of which is shown in Fig. 4) can then be used to generate the modal properties of the bent step index fiber using a variety of techniques [5,10,12,13,25–28]. However, HFs possess a complex transverse structure, and the additional gradient present in the transformed refractive index profile precludes the use of many models. Techniques that are capable of modeling such a complex structure include those based on beam propa-

gation, plane-wave and localized function methods. Whilst techniques based on beam propagation methods (BPM) are capable of accurate representations of the modal properties, they are typically computationally intensive. In the plane-wave approach the modal fields and the refractive index profile are decomposed into plane waves [29–31]. This approach is capable of producing an accurate description of the modal properties if a sufficient number of terms are used in the expansions, but as such can also be computationally intensive. The localized function method follows a similar approach but takes advantage of the fact that the mode(s) of the fiber are localized [32–34]. By using localized functions in the decomposition of the modal field this method requires fewer terms to form an accurate description and as a result can be computationally efficient. Since the modes of the bent fiber are localized for all bend radii of practical interest, we choose this method to model the modal fields of both the straight and bent fiber, as described in the following.

2.2 Modeling the modal properties of straight holey fibers

The model developed in Refs [32–34] is adapted here to calculate the modal properties of straight and bent large mode area HFs. In this model, the transverse refractive index profile and the modal fields are decomposed using orthogonal functions. The transverse refractive index profile is described using a Fourier decomposition with P terms performed over the entire fiber profile. The modal electric field is described using Hermite Gaussian functions using the following approach; the modal electric field is written as;

$$\mathbf{E}_j(x,y,z) = \mathbf{e}_j^t(x,y) + e_j^z(x,y)\hat{\mathbf{z}}\ exp(i\beta_j z) \tag{1}$$

where β_j is the real part of the propagation constant of the jth mode and $\mathbf{e}_j^t(x,y) = e_x\hat{\mathbf{x}} + e_y\hat{\mathbf{y}}$ and e_j^z are the transverse and longitudinal components of the modal electric field, respectively. The transverse modal electric field is then decomposed in terms of localized functions;

$$\mathbf{e}^t(x,y) = \sum_{a,b=0}^{F-1} (\varepsilon_{ab}^x \psi_a(x)\psi_b(y)\hat{\mathbf{x}} + \varepsilon_{ab}^y \psi_a(x)\psi_b(y)\hat{\mathbf{y}}) \tag{2}$$

where F is the number of terms in the expansion and the ψ_a and ψ_b are elements of the following orthonormal set of Hermite-Gaussian basis functions which have a characteristic width (w_m) and are centered on the fiber core:

$$\psi_i(x) = \frac{2^{-i/2}}{\sqrt[4]{\pi}\sqrt{i!w_m}} exp\left(\frac{-x^2}{2w_m^2}\right) H_i\left(\frac{x}{w_m}\right) \tag{3}$$

Here, H_i is the Hermite polynomial of order i. Using these decompositions, the vector wave equation can be reduced to an eigenvalue problem. This problem can be solved numerically for the real part of the propagation constant(s) (β) and the coefficients in the field expansion (ε_{ab}^x and ε_{ab}^y), which are then used to construct the modal field(s) guided by the fiber. Since the basis elements of each decomposition form a complete set, it is possible, in principal, to describe any refractive index profile and modal field with perfect accuracy. However, for the model to be computationally efficient, both decompositions must result in accurate representations of the relevant physical quantities without requiring too many terms. By choosing the number of functions used in each decomposition and the characteristic width (w_m) with care, this technique can be optimized in terms of accuracy and efficiency.

In the large mode area fibers considered here, the holes are small relative to the hole-to-hole spacing ($7.5\mu\text{m} \leq \Lambda \leq 12\mu\text{m}$ and $0.23 \leq d/\Lambda \leq 0.25$) and

so a relatively large number of functions are required in the Fourier decomposition to accurately represent fibers with this large scale difference. In this study, 200 functions are used in the Fourier decomposition (i.e. P=200). For the modal fields, we must consider both the number of functions used in the decomposition (F) and their characteristic width, w_m. If a value of w_m is chosen to suit the particular fiber geometry and operation wavelength, the number of Hermite-Gaussians required can be minimized. For $\Lambda \approx 2\mu$m at a wavelength of 1550nm, a characteristic width of 0.5Λ was found to be optimal [32]. This seems physically reasonable, as the effective mode area should be approximately that of the core. For HFs in which Λ is sub-wavelength, however, the effective mode area can be considerably larger than the core size and w_m must be larger than 0.5Λ. By a similar argument, w_m should ideally be smaller than 0.5Λ for HFs with a large Λ. For the fibers considered here, we have found $w_m = 0.32\Lambda$ to be optimal. For this value of w_m, we find that 12 Hermite-Gaussians are then sufficient to produce a good description of the mode. However, our method of calculating bend loss (described in Section 2.4) is extremely sensitive to the exact shape of the mode and so the accuracy of the modal representation is particularly important. As a result we use 32 Hermite-Gaussians to describe the modal field in this implementation. As an example, Fig. 2(a) shows the calculated intensity profile for the fundamental mode of holey fiber HF1 (Λ = 7.55 μm and d = 1.71 μm) at 1550nm, which has an effective area (A_{eff}) of 140 μm^2 and an effective index (n_{eff}) of 1.44233 (Note that only the central region of the structure used in the calculation is shown). For all predicted values, the effective area is calculated using the definition in Ref. [35].

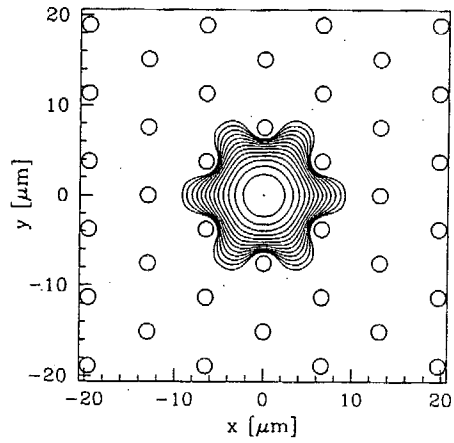

Fig. 2. Calculated modal intensity for holey fiber HF1 at 1550nm. We have used 200 functions in the Fourier decomposition (P) and 32 Hermite-Gaussians (F) with a characteristic width (m_w) of 0.32. Contours are spaced by 1 dB.

Although the full vectorial version is outlined in the above description, we find that in most cases the scalar approximation can be used due to the fact that the fibers in this study possess low values of NA and are only considered in the macro-bend regime (as is demonstrated in Sections 3.2 and 3.4). This is advantageous since we use 32 Hermite-Gaussians in the expansion of the modal field and the numerical simulations are more than an order of magnitude faster for the scalar approximation than those for the fully vectorial approach. However, the vector version is obviously necessary when considering the effect of the polarization of the mode as in Section 3.4.

2.3 Modeling the modal properties of bent holey fibers

To model the modal fields of a bent HF we use the above method together with a conformal transformation, as mentioned in Section 2.1. The conformal transformation is performed before the mode calculation and is used to replace the bent fiber with a straight fiber that has an equivalent refractive index

profile. The equivalent refractive index profile is found by expressing the scalar wave equation in terms of a local coordinate system that follows the curvature of the fiber [27]. (The scalar approximation is valid for the fibers considered here as discussed in Sections 3.2 and 3.4.) A fiber, bent in the y direction for example, can be represented by a straight fiber with an effective refractive index distribution of:

$$n_b{}^2(x,y) = n^2(x,y)(1 + 2y/R_o) \tag{4}$$

where R_o is the radius of curvature and $n(x,y)$ is the refractive index profile of the straight fiber. Thus, by applying the transform in Eq. 4 to the refractive index profile of a straight HF we can define an index profile that mimics the modal properties of a bent holey fiber. For example, the refractive index profile of holey fiber HF1, shown in Figs 3(a) and (b), is transformed using Eq. 4 for a bend radius of 14.5mm, as shown in Fig. 3(c). (Note that only the central region of the structure is shown).

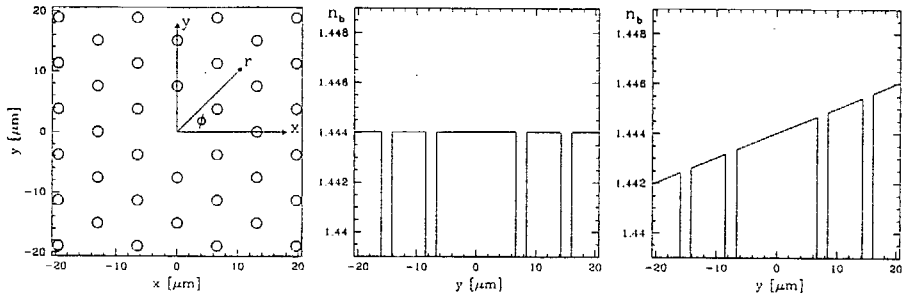

(a) (b) (c)

Fig. 3. (a) Cross-section through center of holey fiber HF1. (b) Transverse slice in the y direction through (a), (c) Transverse slice in the y direction for the refractive index profile in (a) transformed using Eq. 4 for a bend in the y direction, R_o=14.5mm.

These figures show clearly that the transform in Eq. 4 superimposes a gradient onto the refractive index of the straight fiber in the direction of the bend. One

can also see, intuitively, that the mode will distort outwards in the direction of the bend. Furthermore, since the gradient is proportional to the severity of the bend, it is obvious that the mode will become increasingly distorted at tighter bend radii.

Example modal profiles for bent fibers are shown in Fig. 4 for fiber HF1 ($\Lambda = 7.55\mu$m and $d/\Lambda = 0.23$). Figs 4(a) and (b) show the intensity distribution at 1550nm for bends in the x direction of radius 25mm and 19mm respectively. Fig. 4(c) shows slices in the x direction; the solid line corresponds to the mode of the straight fiber (shown in Fig. 2), the dotted line to the mode in Fig. 4(a) and the dashed line to the mode in Fig. 4(b). Similarly, Figs 4(c) and (d) show the intensity distribution at 1550nm for bends in the y direction of radius 25mm and 19mm respectively. Fig. 4(e) shows slices in the y direction; as before the solid line corresponds to the mode of the straight fiber (shown in Fig. 2), the dotted line corresponds to the mode in Fig. 4(c) and the dashed line corresponds to the mode in Fig. 4(d).

These figures show clearly that the mode of the bent fiber is asymmetric in shape and shifts away from the center of the fiber towards the outside of the bend. We can also see that the mode extends further into the cladding and becomes increasingly distorted with decreasing bend radius. The asymmetry in the position and shape of the mode means that the odd terms in the Hermite-Gaussian expansion (odd values of a and b in Eq. 2) become essential in forming an accurate description. Furthermore, this model is designed to be efficient for modes that are localized in the center of the fiber. Indeed, the values stated previously (F=32 and m_w=0.32) were chosen to represent the modal field sufficiently accurately for our bend loss calculations.

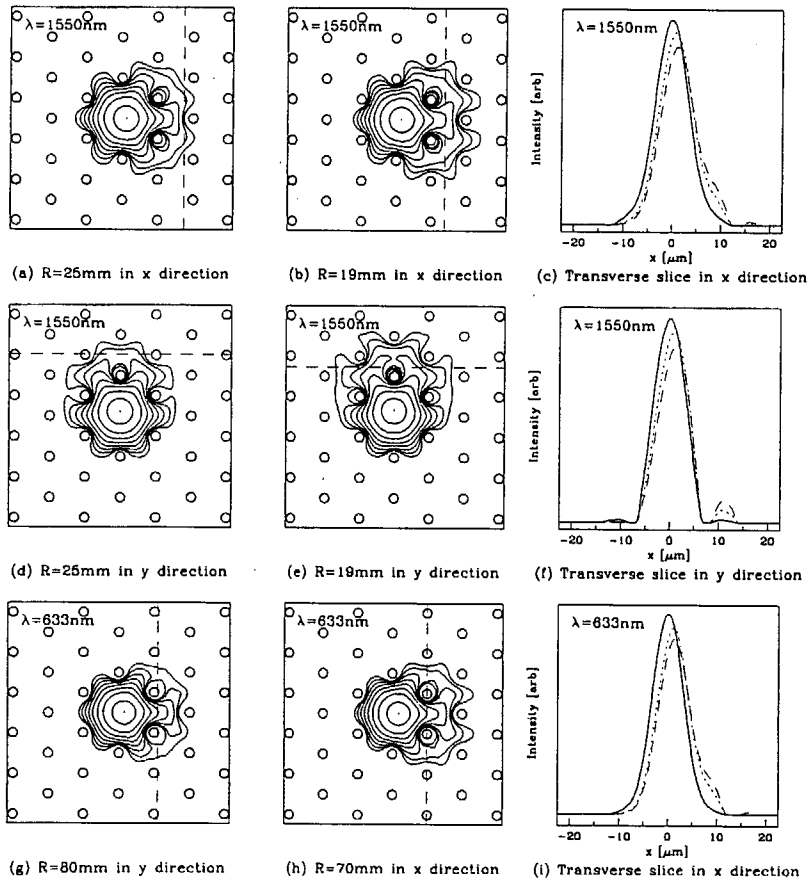

Fig. 4. Parts (a), (b), (d), (e), (g) and (h) show calculated modal intensities for HF1. The contours are spaced by 2dB. The dashed line on each mode profile corresponds to the distance x_r in our model of pure bend loss, defined in Section 2.4.3. Figs (c) and (f) each show three transverse slices along the x and y direction respectively. The solid line in each case corresponds to the mode of the straight fiber at 1550nm (shown in Fig. 2), the dotted line corresponds to the mode in (a) and (d) respectively (R_o = 25mm) and the dashed line corresponds to the mode in (b) and (e) respectively (R_o = 19mm). Fig. (i) shows three transverse slices along the x direction where the solid line corresponds to the mode of the straight fiber at 633nm (not shown), the dotted line corresponds to the mode in (g) (R_o = 80mm) and the dashed line corresponds to the mode in (h) (R_o = 70mm).

Using this approach we are also able to study pure bend loss as a function of wavelength. As mentioned previously, HFs possess a short wavelength bend loss edge in addition to a more conventional long wavelength loss edge. The increase in loss towards short wavelengths results from the fact that the numerical aperture decreases strongly with wavelength, causing the mode to suffer a greater perturbation in response to bending. This is illustrated in the predicted mode profiles shown in Figs 4(g) and (h), calculated for fiber HF1 at 633nm, bent in the x direction for R_o=80mm and R_o=70mm respectively. Indeed, from the transverse cross-sections shown in Fig. 4(i) for the bends at 633nm, and in Fig. 4(c) for bends in the same direction at 1550nm, we can see that the overall degree of mode distortion is similar for the two wavelengths despite the fact that the bend radii are significantly larger for the examples shown at 633nm.

Although the exact refractive index profile of a real HF can be used in this model to calculate the modal fields, we use an idealized index profile, in which measurements of $/Lambda$ and d are extracted directly from a scanning electron microscope image of the real fiber. This is a reasonable assumption for the fibers considered here as the air holes form an almost perfectly regular triangular lattice. The refractive index of silica is taken to be 1.4440236 for a wavelength of 1550nm.

2.4 Modeling the components of bend loss in holey fibers

2.4.1 Overview

As mentioned briefly in Section 1.2, the mechanisms responsible for bend loss involve bend induced coupling from the core mode(s) to radiation modes and also to leaky higher order, cladding and backward propagating modes. For the purposes of this study, we consider only single-moded fibers, ignoring all coupling effects, and we assume that power is lost as radiation from the core mode. In addition, we choose to consider transition loss and pure bend loss separately, as is described in the following two sections.

2.4.2 Transition loss

Transition losses occur where the curvature of the fiber changes suddenly, such as at the beginning and end of a macro-bend. As light travels into the curved fiber, the modal field distorts radially outwards, evolving over some length scale into the mode of the bent fiber. Power is lost in this transition if the length scale is too short for an adiabatic change in mode shape to take place. Here we consider the worst case scenario of an abrupt change of curvature from $R = \infty$ to $R = R_o$ and assume that all power is lost instantaneously to radiation. In this approximation, the transition loss is analogous to a splice loss between the mode of the straight fiber and the mode of the bent fiber, and so the transition loss (in dB) is;

$$\mathrm{TL} = -10\log_{10}\left(\frac{\left|\iint E_o \cdot E_b^*\, dx\, dy\right|^2}{\iint E_o \cdot E_o^*\, dx\, dy \iint E_b \cdot E_b^*\, dx\, dy}\right) \tag{5}$$

where $E_o = E_o(x, y)$ is the field distribution of the straight fiber and $E_b = E_b(x, y)$ is the field distribution of the bent fiber [28].

The assumption that all power is lost as radiation, instantaneously, and the fact that we have ignored mode coupling, overestimates the losses. In reality, power is lost through coupling to higher order, cladding, radiation and backward propagating modes, which is neither an instantaneous or one way process as power can be coupled back into the fundamental mode. Despite this, we can use this method to gauge the order of magnitude of this component of bend loss and to predict trends relating to the fiber design. Since the transition loss is calculated directly from the distorted modal field of the bent fiber, we can also study the effect of the angular orientation of the fiber in the bend.

2.4.3 Pure bend loss

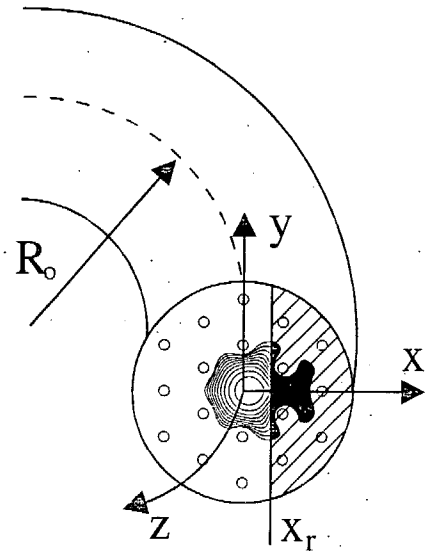

Fig. 5. Mode propagating in the z direction around a bend of radius R_o in the x direction.

Pure bend loss is defined as the continual loss of radiation that occurs along

any curved section of fiber and is related to the inability of the tails of the mode to successfully navigate the bend. The method used here to model the pure bend loss of a holey fiber is based on a method developed for predicting the pure bend loss of slab waveguides [6]. Fig. 5 depicts a guided mode propagating in the z direction around a bend in the x plane that has a radius of curvature R_o. For the mode to propagate along a curved trajectory without suffering loss, the local group velocity along the phase fronts of the mode must decrease on the inside of the bend and increase on the outside of the bend in order to maintain a constant angular velocity across the mode. At some distance towards the outside of the bend (x_r), the required group velocity will exceed the local speed of light. This condition is given by;

$$x_r = \left(\frac{\beta_b}{\beta_c} - 1\right) R_o \tag{6}$$

where β_b is taken to be the propagation constant of the mode of the bent fiber and β_c is the propagation constant of the fundamental mode of the cladding structure. We then assume that the power in the guided mode at $x > x_r$ (f_o) is lost as radiation over some length scale (L), with a power decay rate of;

$$P = P_o e^{-2\alpha z} \tag{7}$$

where P_o is the power in the guided mode before the bend, P is the power in the guided mode at the end of the the bend, z is the length of the curved section, and α is the pure bend loss in units of Np/m (1Np $= -0.5ln(P_{in}/P_{out})$). At $z = L$, the remaining power in the modal field is given by $P = P_o - f_o$. If we substitute this into Eq. 7, we see that $\alpha = (f_o/F_o)/(2L)$, where f_o/F_o is the

fraction of modal power lost and is given by;

$$\frac{f_o}{P_o} = \frac{\int_{-\infty}^{\infty}\int_{x_r}^{\infty} E_b \cdot E_b^* \, dx\, dy}{\int_{-\infty}^{\infty}\int_{-\infty}^{\infty} E_b \cdot E_b^* \, dx\, dy} \tag{8}$$

for a bend in the x direction, where $E_b = E_b(x, y)$ is the modal field of the fiber in the bend. The pure bend loss in units of dB/m is then given by:

$$\text{PBL} = \frac{4.343}{L}\frac{f_o}{P_o} \tag{9}$$

In Ref. [6], it was assumed that the length scale, L, was equal to one Rayleigh range ($L = Z_R$). However, from detailed calculations we find that this choice of L produces an unphysical dependency on mode size. For all waveguides, any increase in the NA results in a more tightly confined mode and so lower bend loss. However, the Rayleigh range decreases rapidly with mode size and so the choice $L = Z_R$ results in larger loss for smaller mode areas, which is unphysical. We propose an alternative length scale based on a simplified ray approach. We assume that the fraction of the modal field beyond $x > x_r$ is no longer guided by the fiber and instead travels along the tangent to x_r, leaving the fiber at the boundary of the microstructured cladding. By this argument, the length scale L is related to the distance between x_r and the intersection of the tangent to x_r and the outermost cladding hole;

$$L = \tau \cdot \sqrt{2R_o(D - x_r)} \tag{10}$$

where D is the distance from the center of the fiber to the outermost hole and τ is a constant of proportionality. Using this approximate ray approach, the predicted bend loss decreases with decreasing mode size as expected. Note that the constant of proportionality τ in effect incorporates a first order correction

to account for mode coupling, which is otherwise ignored in this simplified model.

In Eq. 6 we require the propagation constant of the fundamental mode of the cladding structure (β_c), also known as the fundamental space-filling mode (FSM) [36]. We have found that in order to accurately predict the bending losses, we require knowledge of this parameter correct to at least 7 significant figures. (Changes in the 8th significant figure of β_c produces changes in the 4th significant figure of the pure bend loss, while changes in the 7th significant figure of β_c can lead to changes in the 2nd significant figure of the pure bend loss.) The simplest method of calculating β_c is to find the effective cladding index of an ESI fiber [4]. Unfortunately this method is only approximate since there is no unique choice for the core index and the core radius of the ESI fiber [21]. A more refined analytical method for calculating β_c is proposed in Ref. [37], in which the microstructured cladding is approximated by a unit cell with circular boundaries and periodic boundary conditions. In this study, results for a HF with Λ=2.3μm and d/Λ=0.26 show good agreement with Ref. [30]. However, via comparison with values calculated using a plane-wave method [38], we find that this analytical approach returns values of β_c that are correct only to about 4 significant figures for a range of fiber structures. While this gives a good approximation for β_c, the level of accuracy is well below that which we require in our bend loss calculations.

A better approach is to model the holey fiber cladding directly by considering a structure in which there is no core. One method that can be used to do this is the Multipole approach [39], in which the modal fields are calculated using decompositions based on cylindrical harmonic functions localized in each of the cladding holes. This method is capable of producing accurate, complex values

of β_c for a finite cladding structure. However, it is necessary to consider the entire extent of the fiber in this approach and is, as a result, computationally intensive. The plane-wave method, as discussed briefly in Section 2.1, is also capable of producing accurate values of β_c [30,36]. Whilst this technique can be computationally intensive, we need only model a single unit cell in order to calculate the properties of the FSM for an infinite cladding structure composed of a perfectly regular lattice. In this way we can calculate β_c for an infinite cladding both efficiently and accurately. Here we choose to use a commercially available software package called bandSOLVE^{TM}, which is based on a plane wave approach, to calculate β_c.

Example calculations and other insights

In Fig. 4 example modal profiles for fiber HF1 ($\Lambda = 7.55\mu$m and $d/\Lambda = 0.23$) are shown for various bend radii and directions at 1550nm and 633nm. In this section we describe the bend loss calculations for some of the cases shown in Fig. 4 and highlight some of the main trends predicted by our model of pure bend loss. The critical point (x_r) beyond which all power is lost as radiation is defined in Eq. 6 and depends only on the propagation constant of the mode of the bent fiber (β_b), the propagation constant of the FSM of the straight fiber (β_c) and the bend radius (R_o). The location of x_r is indicated on each plot in Fig. 4 by a dashed line. For HF1 at 1550nm, $\beta_c = 5.844182 \times 10^6$. For a bend of R_o=25mm in the $\phi = 0^o$ direction (Fig. 4(a)), $\beta_b = 5.846873 \times 10^6$ and so $x_r = 11.5\mu$m, which equates to 3% of the mode lost as radiation. For a bend of R_o=19mm in the $\phi = 0^o$ direction (Fig. 4(b)), $\beta_b = 5.847015 \times 10^6$ and $x_r = 9.2\mu$m, which equates to 10% of the mode lost as radiation. These

results demonstrate that the predicted bend loss increases with decreasing bend radius as expected. In addition, we can show that the bend loss increases towards short wavelengths in this fiber type. For the larger bend radii of 80mm and 70mm at 633nm (Figs 4(g) and (h) respectively), the fraction of the mode lost as radiation is 9% for a bend radius of 80mm and 15% for a bend radius of 70mm, thus confirming the presence of the short wavelength loss edge.

3 Experimental and comparison with theory

3.1 Overview

This section presents the results from an experimental study of bend loss in HFs. We have investigated bend loss as a function of the radius of curvature, the relative contributions of transition and pure bend loss, and the effect of the the angular orientation of the fiber in the bend. Where applicable we also present the results from our theoretical predictions. Unless otherwise stated, all spot values of pure bend loss for HF1 are calculated using the full vector version of the modal model described in Section 2.2.

In all of the following experiments, care was taken to ensure that any change in fiber curvature was well defined. Care was also taken to exert minimal tension on the fiber and to ensure that the fiber lay flat along its entire length. These precautions ensure that the measured loss can be attributed purely to the regions of curvature that are deliberately imposed along the length of fiber and not from any other minor perturbations in the straight fiber regions, ensuring a robust and repeatable method of measurement. In the following experiments, light is coupled into the fibers under characterization from a

single-mode fiber laser with a pair of aspheric lenses. The bend loss is defined as the ratio between the power transmitted through the straight fiber and the bent fiber, expressed in dB.

3.2 Bend loss as a function of radius of curvature

Loss was measured at 1550nm as a function of the bend radius for fibers HF1-3. These measurements were taken for one circular loop of fiber, ensuring that there was a sharp change of curvature at the beginning and end of the loop, as mentioned above. These measurements were repeated for several random angular orientations of the fiber and are shown in Figs 6(a), (b) and (c), by the open shapes. Superimposed on each graph is a curve fitted to all the experimental data for each fiber. This enables us to average over the different angular orientations and thus extract an average value for the critical radius R_c, defined as the radius at which the loss is equal to 3dB for one loop of fiber. This critical radius is found to be 21mm, 46mm and 66mm for holey fibers HF1, HF2 and HF3 respectively, which increases with mode size as expected.

In order to understand the relative contributions that transition loss and pure bend loss make to the net observed loss, we now compare these results with our theoretical predictions. For one full loop of fiber, there are two transition regions, one at the beginning of the bend and another at the end of the bend, which result in two transition losses. Figs 7 (a), (b) and (c) show the measured bend loss for fibers HF1, HF2 and HF3, as in the previous graph, together with predicted values for the transition loss and pure bend loss. The dotted lines in Figs 7 (a), (b) and (c) show the predicted transition loss for one full loop of fiber bent in the $\phi = 0°$, 45° and 90° directions for HF1, HF2 and HF3

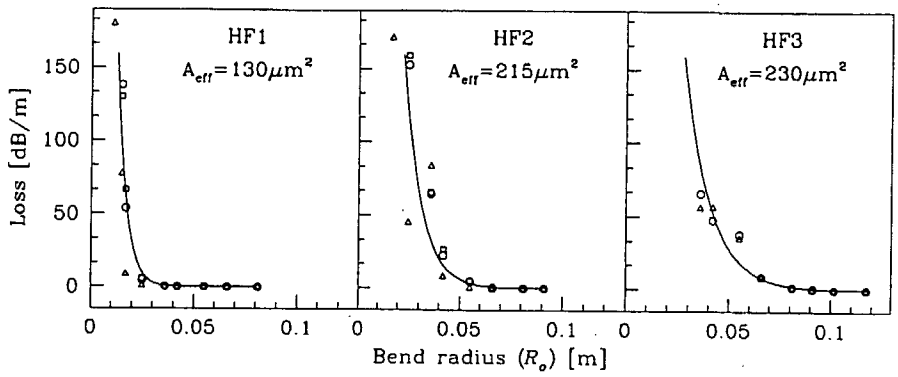

Fig. 6. Loss for one loop of fiber as a function of bend radius. Open shapes represent measured bend loss for (a) HF1, (b) HF2 and (c) HF3 for different random angular orientations of the fiber. The solid line in each graph corresponds to the fitted curve from which the critical radius is extracted.

respectively. These predicted values clearly show that transition loss is a small overall contribution to bend loss for these HFs in the macro-bend regime at 1550nm and implies that the majority of loss must be attributed to pure bend loss.

The predicted pure bend loss is shown for each fiber by the solid lines in Figs 7(a), (b) and (c) for bends in the $\phi = 0°$, 45° and 90° directions. Recall that in our model of pure bend loss, a constant of proportionality (τ) was introduced in Eq. 10. Since the transition loss is a small contribution to the overall loss (Fig. 7), this factor can be found by fitting the predicted curves to the experimental data. We find that by choosing $\tau = 6$, we achieve excellent agreement with experimental data for all three fibers, as can be seen in Figs 7(a), (b) and (c). For example, using our scalar model, the critical bend radius (R_c), is predicted to be 23mm, 44mm and 58mm for holey fibers HF1, HF2 and HF3 respectively. This compares well with experimental values of R_c (given above) of 21mm, 46mm and 66mm for holey fibers HF1, HF2 and HF3 respectively. Note that by using the vectorial method to calculate the modal

fields of HF1 the value of the critical radius changes slightly to R_c = 24mm. These results show that the scalar approximation provides a useful method for predicting the critical radius and enables us to efficiently gauge the bend radii over which any given fiber is practical to use.

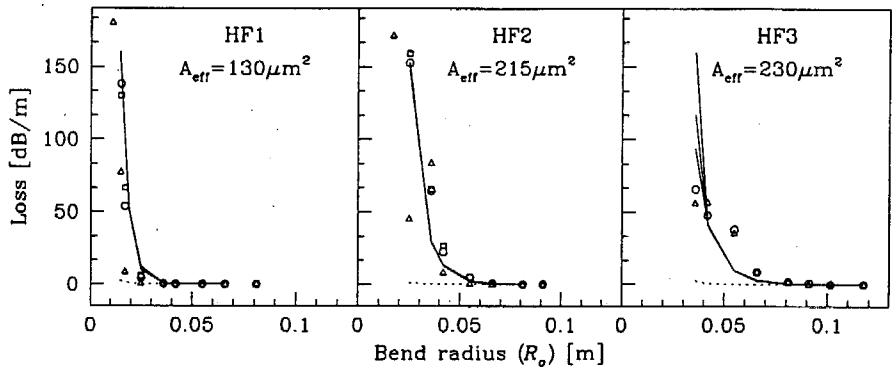

Fig. 7. Loss as a function of bend radius. Open shapes represent measured bend loss for (a) HF1, (b) HF2 and (c) HF3 for different random angular orientations of the fiber, while the predicted pure bend loss is shown by solid lines for bends in the ϕ = 0°, 45° and 90° direction. The predicted transition loss is shown by dotted lines for bends in the ϕ = 0°, 45° and 90° direction.

3.3 Distinguishing transition loss and pure bend loss experimentally

In this section, the relative contributions of transition loss and pure bend loss are separated experimentally to explicitly test our theoretical predictions that transition loss is dominated by pure bend loss. The experiment shown in Fig. 8(a) was designed in Ref. [9] to distinguish transition and pure bend loss in conventional step index fibers. In this experiment, a length of fiber is progressively wrapped around a drum of radius R_o by rotating the stage carrying the detector. The fiber is carefully supported at points A and B with straight guides to produce a sharp change in curvature without inducing any unwanted stresses on the fiber. The guide at point A remains fixed and it is

extremely important for the guide at B to reproduce the same sharp change in curvature as the fiber is wrapped around the drum. The fiber chuck and fiber chuck rotator, which enabled the angular orientation of the fiber to be controlled with an accuracy of half a degree, are also shown in Fig. 8(a).

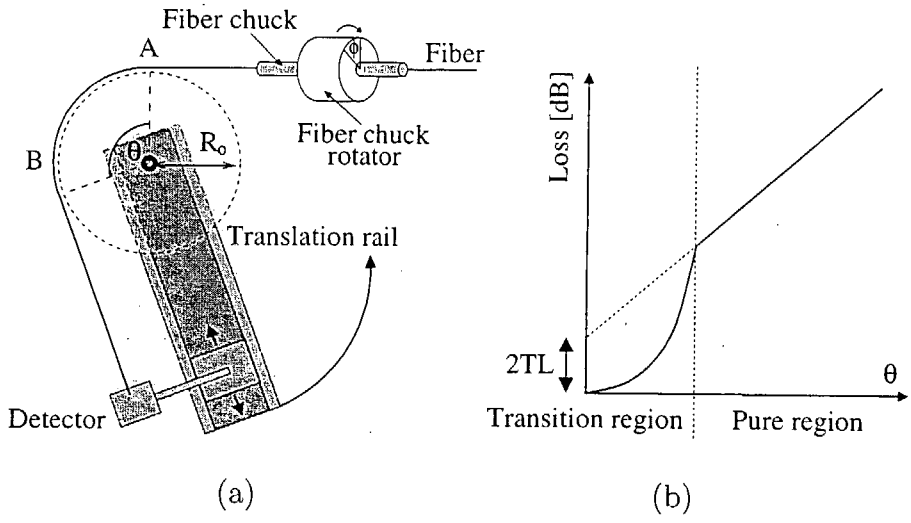

Fig. 8. (a) Experimental set-up to observe transition loss and pure bend loss in a bent optical fiber. Loss is measured as the fiber is progressively wrapped around a drum of radius R_o (The wrap-around angle = θ). The fiber chuck and rotator are used to control the angular orientation (ϕ) of the fiber in the bend. (b) Schematic of results.

Fig. 8(b) shows a sketch of typical results. Transition losses occur at the points A and B where there is a sharp change in curvature from $R = \infty$ to $R = R_o$ and back again. These transition losses (TL) take place over a finite length of fiber, as shown by the curved section in graph Fig. 8(b). The length of fiber between points A and B is of constant curvature and suffers a continuous pure bend loss along its entire length. As the wrap-around angle (θ) is increased, the length of the curved section of fiber (and the pure bend loss) increases linearly. The pure bend loss can be extracted from the gradient of the straight line section of the graph in Fig. 8(b), which is offset by the two transition

losses at the beginning and end of the bend. The transition loss can then be extrapolated from the graph as sketched in Fig. 8(b).

This experiment was performed for the conventional fiber C1 ($A_{eff} = 126\ \mu m^2$ at 1550nm) and the similarly sized holey fiber HF1 ($A_{eff} = 130\ \mu m^2$ at 1550nm) to enable comparisons to be drawn between the two fiber types. For each fiber, the loss was measured as a function of θ for a fixed radius of curvature. A radius of 14.5mm was chosen to ensure that the loss due to mode deformation was sufficiently large enough for the transition region to be clearly visible.

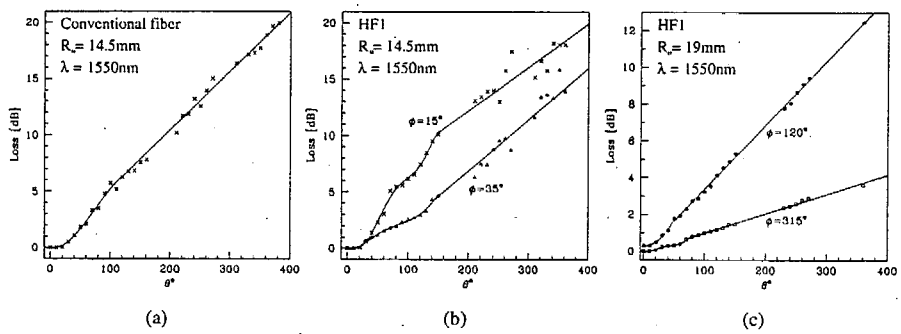

Fig. 9. Results from experiment shown in Fig. 8 for $\lambda = 1550$nm (a) conventional fiber C1, R_o=14.5mm, (b) holey fiber HF1, R_o=14.5mm, (c) holey fiber HF1, R_o=19mm.

Figs 9(a) and (b) show the measured loss at 1550nm for R_o=14.5mm as a function of angle for the conventional fiber C1 and holey fiber HF1 respectively, together with fitted curves drawn to guide the eye. Unsurprisingly, we find that the overall loss values for HF1 are similar in magnitude to those of the similarly sized conventional fiber C1. In addition, we find that, for both fiber types, two regions of loss can be distinguished: the curved section at small values of θ is the transition region, while pure bend loss dominates as the length of the bent fiber is increased. As expected, we find that a linear fit can be used to describe the pure bend loss region. For the case of holey fiber HF1,

data sets are shown that correspond to two different angular orientations of the fiber relative to the bend (see Fig. 9(b)). These two data sets demonstrate that both the transition loss and the pure bend loss depend strongly on the orientation of the HF relative to the bend. Notice also that the shape of the curve in the transition region for holey fiber HF1 is more complex than that of the conventional fiber, which may reflect the more complex spatial modal field distribution of a bent HF.

The pure bend loss for one loop of fiber, extracted from the slope of the linear fit to the pure bend loss regions in Figs 9(a) and (b), is found to be 19.4dB for the conventional fiber C1 and 14.0dB and 16.6dB for the different orientations of holey fiber HF1 for R_o=14.5mm. The range of values measured here for HF1 compare well with predicted values of pure bend loss, which range between 13.9dB and 16.8dB depending on the angular orientation of the fiber and the polarization of the mode. (The variation in bend loss as a function of angular orientation and polarization is discussed in more detail in Section 3.4.)

The transition loss for R_o=14.5mm, extracted from the y intercept of the straight line fit, is found to be approximately 0.06 dB for the conventional fiber C1 and 4.5dB and -2.2dB for the different orientations of the holey fiber HF1. This latter, apparently unphysical, result may arise from the assumption that the pure bend loss is constant within the transition regions at the beginning and end of the bend. This is true only if the mode of the straight fiber transforms into the mode of the bent fiber instantaneously. From the width of the transition region in Figs 9(a) and (b) we can see that this is not the case. As mentioned previously, on entering the bend, the modal field evolves, over some length scale, into the mode of the bent fiber, which extends further into the cladding in the direction of the bend. In the initial stages of distor-

tion, the pure bend loss will thus be less than for the fully distorted mode. By assuming a constant value of pure bend loss within the transition region, we underestimate the transition loss from the intercept of the straight line fit to the pure bend loss region. From this argument, we can see that the y intercept of the straight line fit to the pure bend loss region may be negative, if the mode distortion is significant. For fiber HF1 at 1550nm, with a bend radius of 14.5mm, the overall predicted transition loss is equal to 2dB, which is approximately consistent with the experimentally derived values. Although this value is still small when compared to the pure bend loss, it is significantly higher than the measured transition loss for the similarly sized conventional fiber C1 for R_o=14.5mm.

Results for R_o = 19mm for fiber HF1 at 1550nm are shown in Fig. 9(c) and demonstrate that for this larger bend radii and lower overall loss, the transition region is relatively less pronounced. The two data sets shown here were chosen to correspond with the maximum and minimum observed loss orientations. The pure bend loss for one loop of fiber, extracted from the slope of the linear fit to the pure bend loss regions in Fig. 9(c) are 4.0dB and 12.6dB for the different orientations of holey fiber HF1. Again, this shows good agreement with our predicted values for pure bend loss, which are found to be between 6.6dB and 7.7dB for one loop of fiber, depending on the angular orientation of the fiber and the polarization of the mode.

We also briefly investigated the effect of the short wavelength loss edge. Since the midpoint between the long and short wavelength loss edges has empirically been shown to be $\Lambda/2$ [16], we expect that the bend loss for all wavelengths below 1550nm should increase, despite the fact that the mode size decreases (A_{eff} = 130 μm^2 at 1550nm and A_{eff} = 70 μm^2 at 633nm). This was confirmed

experimentally by measuring the bend loss of fiber HF1 at 633nm, using the set-up shown in Fig. 8 for the two angular orientations shown in Fig. 9(b) (R_o=14.5mm, data not shown here for reasons of brevity). As expected, we find that the losses at 633nm are considerably higher than for this same bend radius at 1550nm, shown in Fig. 9(b). The components of loss, extracted from a straight line fit to the pure bend loss region, yield values of 9dB for two transition losses and 50dB for one full loop of fiber. Although the transition loss is still a small overall contribution to the overall loss, it is relatively higher than for the same fiber and bend radius at 1550nm. In addition, we also find that there is no significant difference in the bending losses for the two angular orientations of fiber, which correspond to the maximum and minimum loss orientations found at 1550nm. Recall that our predictions show that for a given bend radii, the modal field suffers a greater distortion at 633nm relative to 1550nm, increasing the modal field intensity close to the boundary of the microstructured cladding. As a result, we may expect the variation in loss as a function of angular orientation to increase at 633nm relative to 1550nm. This is something that obviously warrants further investigation, but is not considered in any more detail here.

In the next section, we investigate the effect of the geometry of the cladding structure on the bend loss characteristics at 1550nm in more detail.

3.4 Bending losses in holey fibers as a function of angular orientation

For the HFs considered here, we have shown that the measured bend loss varies as a function of the angular orientation of the fiber in the bend (see for example Fig. 9). In this section we look at this in more detail using both

experimental and theoretical techniques.

In Fig. 10 the predicted pure bend loss is shown for holey fiber HF1 as a function of bend radius. For each bend radius, the loss is shown for bend directions of $\phi = 0°$, $45°$ and $90°$, calculated using both the scalar and vector version of the modal model described in Section 2.2. The relationship between the bend loss, the bend direction and the polarization of the mode is complex, and for simplicity we highlight the main trends shown in Fig. 10. We can clearly see that the variation in bend loss for any given bend radii increases as the bend becomes tighter. In addition, we find that for those bends that are tighter than the critical radius, the variation in loss can be mainly attributed to the different polarizations of the mode. Conversely, for those bends that are larger than the critical radius, the loss variation is greatest for the different bend directions, and influence of the mode polarization is small. Note also that while the results calculated using the scalar version of the modal modal in Section 2.2 predict a smaller variation in loss with respect to the angular orientation of the fiber in the bend, the average loss values agree well, demonstrating that the scalar version is perfectly adequate for a practical estimation of R_c.

From previous experiments we have seen that the observed variation in loss agrees well with predicted values for pure bend loss. However, in the results presented in Section 3.3 only a few angular orientations of the fiber were considered. To evaluate the relationship between bend loss and the angular orientation of the fiber in a more systematic manner, we used the experimental set-up shown in Fig. 8. The wrap-around angle θ was fixed at 130° and the loss was measured as a function of angular orientation (ϕ) for holey fiber HF1 for a fixed bend radius of 14.5mm and 19mm at 1550nm. A wrap-around angle of 130° was chosen so that the majority of loss could be attributed to pure

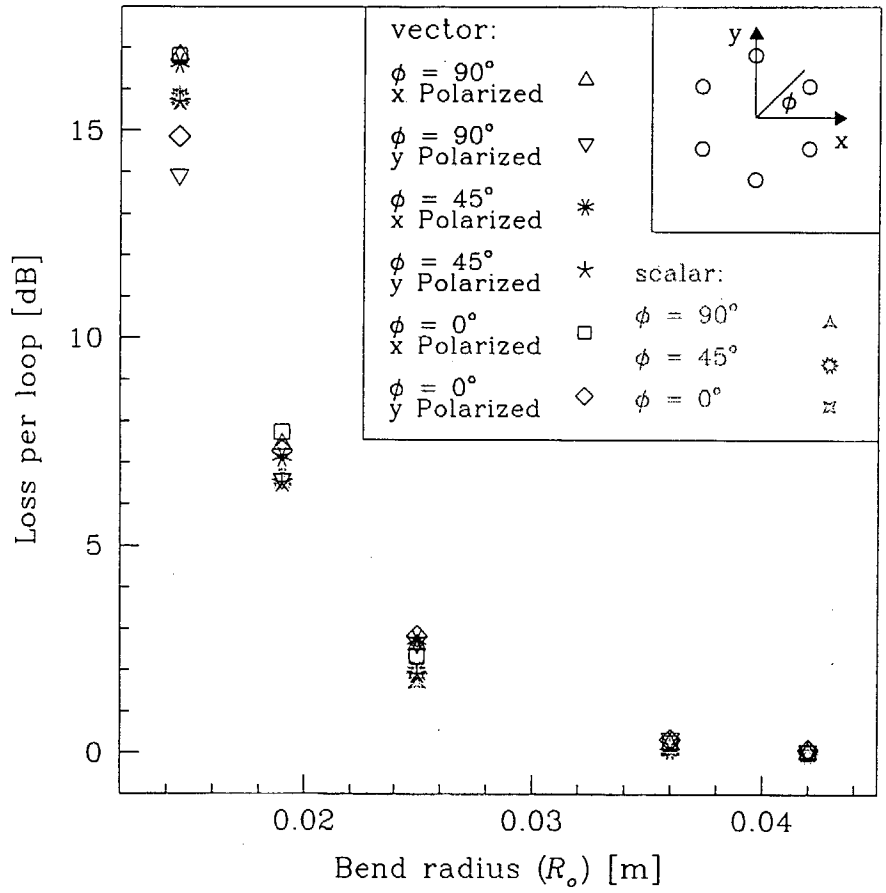

Fig. 10. Predicted pure bend loss as a function of bend radius for HF1 at 1550nm for different bend directions (ϕ) and polarization states as indicated on the figure.

bend loss without the overall loss value being too severe. The resulting loss curve for $R_o = 14.5$mm (not shown here for brevity) shows a variation in loss with angular orientation that is equivalent to a loss of 41.5dB in one full loop of fiber, with a minimum loss of 5.5dB and an average loss approximately equal to 19dB for one loop. This value, averaged over 160 equally spaced angular orientations, agrees well with our predicted values of pure bend loss, which range between 13.9dB and 16.8dB depending on the angular orientation of the fiber and the polarization of the mode (from Fig. 10). However, the observed variation in loss per loop is far greater than predicted by theory; 41.5dB compared to the predicted value of 2.9dB.

Similarly, we find that for a bend radius of 19mm, the average observed loss values agree well with predictions, but the degree of variation does not. Measured values of bend loss vary between 4.0dB and 12.6dB, with an average value (averaged for 11 equally spaced values of ϕ) of 8.7dB for one loop of fiber, while predicted values vary from 6.6dB to 7.7dB for one loop of fiber.

In order to understand this apparent discrepancy between the observed variation in loss and our theoretically derived values, we investigated how the cladding structure of the fibers used here differs from the idealized fiber profile used in our theoretical calculations. One obvious difference is the slightly irregular nature of the outer boundary of the microstructured cladding, which results from the fact that the positions of the air holes deviate from the perfect lattice in the 3 outermost rings of holes. Furthermore, in all of the fibers used here, the core is offset from a central position by one lattice point and results in the fact that the extent of the cladding (D) varies from seven to eight rings of holes around the core. Unfortunately, the loss curves for HF1 as a function of angular orientation at 14.5mm and 19mm (both not shown here) have a complex shape, and it is difficult to correlate the measured loss values with any of the features discussed above. However, we find that by increasing the bend radius and thus decreasing the overall loss values, it becomes easier to distinguish the effects of some of the cladding features.

The bend loss was measured as a function of the angular orientation of the fiber for holey fiber HF4, which is larger in scale than HF1 (parameters shown in Table 1), but has an almost identical cladding configuration. A bend radius of 30.5mm was chosen for this fiber to achieve low overall bending losses so that the effects of the cladding might be more clearly distinguished. Fig. 11(a) shows loss as a function of angular orientation for HF4 for a wrap-around angle

of 130° and a bend radius of 30.5mm at 1550nm. Fig. 11(b) shows 1/D as a function of angular orientation, where D is defined as the distance from the center of the core to the center of the outermost hole in the cladding. We can see that these two graphs strongly correlate, with the region of minimum loss coinciding with the direction in which the extent of the cladding is greatest and the maximum region of loss coinciding with direction in which the outermost hole is closest to the core. Indeed, these results show that for this radius, one additional ring of holes in the cladding can reduce the loss by approximately 1.5dB for a wrap-around angle of 130°, which is equivalent to a reduction of 20dB/m. In addition to the overall shape of the two curves, we can also see that some of the sharp features in the shape of the cladding boundary are reflected in the loss curve. For example, around 140° and between 200° and 230° sharp increases in loss can be seen to correspond to holes in the outermost cladding that are closer to the core than their neighbors. This demonstrates that both the overall extent of the cladding and the shape of the boundary are important factors in determining the bend loss and must be considered in the design of future HFs.

4 Discussion and conclusion

In high power fiber applications, large mode areas are required in order to avoid damage to the fiber and to minimize non-linear effects that would otherwise distort the signal. Holey fiber technology is an attractive alternative to conventional technology, since it is possible to create extremely large mode area fibers that are single-moded over a broad wavelength range. Indeed, HFs with effective areas as large as $680\mu m^2$ at 1550nm have been demonstrated

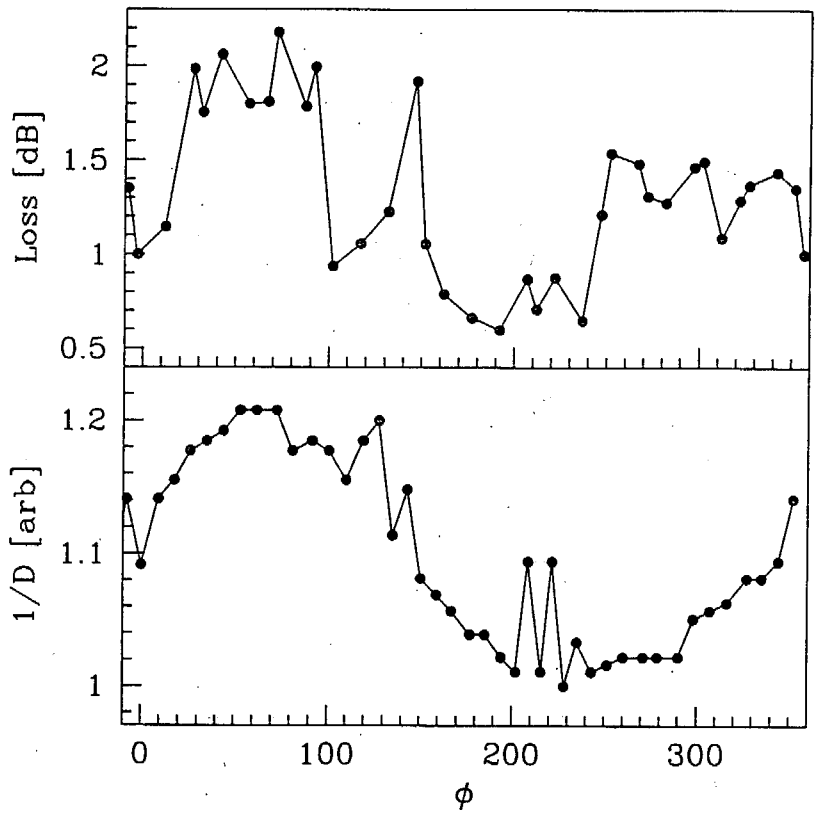

Fig. 11. (a) Loss as a function of angular orientation for holey fiber HF4 R_o=30.5mm (b) 1/D as a function of angular orientation for holey fiber HF4 where D = distance from the center of the core to the outermost hole in the cladding.

that are effectively endlessly single-mode [1]. However, as with any fiber, the macro-bending losses place a fundamental upper limit on the mode sizes that are practical to use and are therefore an important consideration in the design of large mode area fibers. Currently, knowledge of the factors that influence bend loss in HFs is limited and there has been little development towards theoretical techniques that could be used to design HF structures with greater resistance to bending. In this study we have investigated bend loss in HFs, and have increased our understanding of the factors that influence these losses. Most importantly, we have developed a method that can be used to predict

the critical bend radius of large mode HFs both accurately and efficiently.

The theoretical approaches to bend loss presented here are adapted from methods previously developed for conventional waveguides and, importantly, do not assume a circularly symmetric refractive index profile. These methods do, however, require that both the modes of the straight and bent fiber be known. Here we choose to calculate the modes of the straight and bent fiber using a model adapted from Ref. [33]. In the case of the bent fiber, we first apply a well known transform to the refractive index profile of the bent fiber, which then allows the mode of the bent fiber to be calculated in the same way. Once the modal fields of the fiber are known, we calculate the transition loss as a splice loss between the mode of the straight fiber and the distorted mode of the bent fiber. The pure bend loss is calculated by evaluating the fraction of the modal field in the bent fiber that has to travel faster than the local speed of light to negotiate the bend. These techniques enable us to predict the transition losses and the pure bend losses for any HF, using the full refractive index profile, and for any given angular orientation of bend. Using these theoretical methods we have demonstrated excellent agreement with experimentally derived values.

Results from an experiment designed to separate the components of bend loss, performed for different bend radii and for different wavelengths, show, unsurprisingly, that both components of bend loss increase as the bend radius is reduced. In addition, by comparing results for different wavelengths we see that both the transition loss and the pure bend loss increase towards short wavelengths, despite the fact that the mode area decreases, demonstrating the presence of the short wavelength bend loss edge. These relationships are correctly predicted by our models for transition loss and pure bend loss as the mode of the bent fiber becomes increasingly distorted with decreasing

bend radii and wavelength. In addition, both our experimental observations and our theoretical predictions show that the transition loss is a small overall contribution to macro-bend loss in the HFs considered here and that the bend loss for one full loop of fiber can be well approximated by pure bending losses only, as in conventional fibers. Indeed, our model of pure bend loss predicts the critical radius to within 4-12% of the observed value for the three fibers considered in here.

An important difference between conventional and holey fibers is the complex nature of the transverse refractive index profile. Previous work on bending losses in HFs has ignored the effect of the complex fiber structure for simplicity. While our theoretical results predict that any variation in loss as a function of angular orientation of the fiber in the bend is small, in practice, we observe that the bend loss can vary strongly as a function of angular orientation for the fibers considered here. We have shown that this variation in loss is directly related to the extent of the cladding and, more specifically, to the distance from the center of the core to the outermost hole (for the fibers considered here, the core is offset by one lattice point). The fact that this relatively subtle deviation from a perfect structure is so strongly reflected in the bend loss indicates that the structure of the outer cladding is an important consideration in large mode area HF design. This variation in bend loss results from the fact that the confinement of the bent mode is strongly dependent on the extent of the cladding. Due to the fact that the model used here to calculate the modal fields of the bent fiber uses periodic boundary conditions, we are not able to model the confinement losses of the distorted mode that are associated with a finite holey cladding. Two obvious methods that could be used to study these effects in HFs include the Multipole approach and various BPM techniques.

However, BPM techniques are typically computationally intensive and the Multipole approach is not capable of modeling the mode of a bent HF using the transformation in Eq.4, since it assumes a constant background refractive index [39].

In conclusion, we have developed experimental techniques that have enabled us to characterize the basic components of bend loss in large mode area holey fibers. We have developed and experimentally validated theoretical approaches that retain the full refractive index profile and include the effect of the angular orientation of the cladding. Together, these techniques present us with powerful tools that can be used to study the bending losses of any large mode area HF, which is essential in the task of developing HF structures with greater resistance to bending. It should also be noted that the theoretical techniques outlined here are also applicable to higher order modes. Since the bending losses of higher order modes are significantly greater than the fundamental mode, it may be possible to design HF structures that are *effectively* single-moded for certain bend radii. In addition, since there are few restrictions regarding the refractive index profile that can be modeled, these methods are also applicable to conventional fibers and to HF profiles that include doped regions or more complex hole arrangements.

References

[1] J.C.Baggett, T.M.Monro, K.Furusawa, D.J.Richardson, Comparative study of bend loss in large mode holey and conventional fibers, Opt. Lett. **26** (14) (2001) 1045–1047.

[2] J.C. Knight, T.A. Birks, R.F. Cregan, P.St.J. Russell and J.P.de Sandro, Large mode area photonic crystal fiber, Elect. Lett. **34** (13) (1998) 1346–1347.

[3] J.C.Knight, T.A.Birks, P.St.J.Russell, D.M.Atkin, All-silica single-mode optical fiber with photonic crystal cladding, Opt. Lett. **21** (19) (1996) 1547–1549.

[4] T.A. Birks, J.C. Knight, and P.St.J. Russell, Endlessly single-mode photonic crystal fiber, Opt. Lett. **22** (13) (1997) 961–963.

[5] W.A. Gambling, H. Matsumura and C.M. Ragdale, Curvature and microbending losses in single-mode fibers, Opt. and Quant. Elect. **11** (1979) 43–59.

[6] E.A. Marcatili and S.E. Miller, Improved relations describing directional control in electro-magnetic wave guidance, The Bell Sys. Tech. J., September 1969 2161–2188.

[7] M. Heiblum and J.H. Harris, Analysis of curved optical waveguides by conformal transformations, IEE J. Quant. Electron. **11** (2) (1975) 75–83.

[8] W.A. Gambling, H. Matsumura and R.A. Sammut, Mode shift at bends in single-mode fibers, Elec. Lett. **13** (23) (1977) 695–697.

[9] W.A. Gambling, H. Matsumura, C.M. Ragdale and R.A. Sammut, Measurement of radiation loss in curved single-mode fibers, Micro. Opt. and Acoust. **2** (4) (1978) 134–140.

[10] J. Saijonmaa and D. Yevick, Beam propagation analysis of loss in bent optical waveguides and fibers, J. Opt. Soc. Am. A **73** (12) (1983) 1785–1791.

[11] A.J. Harris and P.F. Castle, Bend loss measurements on high numerical aperture small mode fibers as a function of wavelength and radius of curvature, J. Lightw. Tech. **4** (1) (1986) 34–40.

[12] J. Yamauchi, M. Ikegaya and H. Nakano, Analysis of bent step index fibers by the beam propagation method, IEE Proc. J. Optoelect. **139** (3) (1992) 201–207.

[13] M. Mirianashvili K. Ono and M. Hotta, Coupled mode analysis of loss in single-mode bent optical fibers, Jpn. J. Appl. Phys. **39** (2000) 1468–1471.

[14] W. Berglund and A. Gopinath, WKB analysis of bend loss in optical waveguides, J. Lightw. Tech. **18** (8) (2000) 1161–1166.

[15] D. Donlagic and B. Culshaw, Propagation of the fundamental mode in curved graded index multimode fiber and its application in sensor systems, J. Lightw. Tech. **18** (3) (2000) 334–342.

[16] T. Sorensen, J. Broeng, A. Bjarklev, E. Knudsen and S.E. Barkou Libori, Macro-bending loss properties of photonic crystal fiber, Elect. Lett. **37** (5) (2001) 287–289.

[17] K. Furusawa, T.M. Monro, P. Petropoulos, and D.J. Richardson, A mode-locked laser based on ytterbium doped holey fiber, Elect. Lett. **37**(9) (2001) 560–561.

[18] M. Artilia, G. Coppa, P.Di Vita, M. Potenza and A. Sharma, Mode field diameter measurements in single-mode optical fibers, J. Lightw. Tech. **7** (8) (1989) 1139–1152.

[19] http://syllabus.syr.edu/ELE/kdl/Ele682/smf28.PDF

[20] T. Sorensen, J. Broeng, A. Bjarklev, E. Knudsen, S.E. Barkou Libori, H.R. Simonsen and J.R. Jensen, Macrobending loss properties of photonic crystal fibers with different air filling fractions, Proc. 27th European Conference on optical communications (ECOC' 2001), We.L2.4 (2001).

[21] J.Rishede, S.B.Libori, A.Bjarklev, J.Broeng and E.Knudsen, Photonic crystal fibers and effective index approaches, Proc. 27th European Conference on optical communications (ECOC' 2001), TH.A1.5 (2001).

[22] W.A. Gambling and H. Matsumura, Propagation characteristics of curved fibers, Trans. IECE Japan **E61** (1978) 196–201.

[23] D. Marcuse, Curvature loss formula for optical fibers, J. Opt. Soc. Am. A **66** (3) (1976) 216–220.

[24] J. Sakai and T. Kimura, Bending loss propagation in arbitrary-index profile optical fibers, Appl. Opt. **17** (10) (1978) 1499–1506.

[25] Hagen Renner, Bending losses of coated single-mode fibers: a simple approach, J. Lightw. Tech. **10** (5) (1992) 544–551.

[26] L. Faustini and G. Martini, Bend loss in Single-Mode Fibers, J. Lightw. Tech. **15** (4) (1997) 671–679.

[27] D. Marcuse, Influence of curvature on the losses of doubly clad fibers, Appl. Opt. **21** (23) (1982) 4208–4213.

[28] W.A. Gambling, H. Matsumura and C.M. Ragdale, Field deformation in a curved single-mode fiber, Elect. Lett. **14** (5) (1978) 130–132.

[29] E. Silvestre, M.V. Andrés, and P. Andrés, Biorthonormal-basis method for the vector description of optical-fiber modes, J. Lightw. Tech. **16** (5) (1998) 923–928.

[30] A. Ferrando, E. Silvestre, J.J. Miret, P. Andrés and M.V. Andrés, Full-vector analysis of a realistic photonic crystal fiber, Opt. Lett. **24** (5) (1999) 276–278.

[31] S.G. Johnson and J.D. Joannopoulos, Block-iterative frequency-domain methods for Maxwell's equations in a planewave basis, Opt. Exp. **8** (3) (2001) 173–190. http://www.opticsexpress.org/abstract.cfm?URI=OPEX-8-3-173

[32] T.M. Monro, D.J. Richardson, N.G.R. Broderick and P.J. Bennett, Holey optical fibers: an efficient modal model, J. Lightw. Tech. **17** (6) (1999) 1093–1102.

[33] T.M. Monro, D.J. Richardson, N.G.R. Broderick and P.J. Bennett, Modeling large air fraction holey optical fibers, J. Lightw. Tech. **18** (1)(2000) 50–56.

[34] T.M. Monro, N.G.R. Broderick and D.J. Richardson, Exploring the optical properties of holey fibers, *Nanoscale, linear and nonlinear optics,* International School on quantum Electronics Erice, Sicily (2000). Ed: M. Bertolotti, C.M. Bowden and C. Sibilia, AIP conference proceedings **560**.

[35] Govind P. Agrawal, *Nonlinear Fiber Optics*, 3^{rd} Ed. Academic Press (1995).

[36] Z. Zhu and T.G. Brown, Analysis of the space filling modes of photonic crystal fibers, Opt. Exp. **8** (10) (2001) 547–554. http://www.opticsexpress.org/abstract.cfm?URI=OPEX-8-10-547

[37] Michele Midrio, Mukesh P. Singh and Carlo G. Someda, The space filling mode of holey fibers: an analytical vectorial solution, J. Lightw. Tech. **18** (7) (2000) 1031–1037.

[38] N.A. Mortensen, M.D. Nielsen, J.R. Folkenberg, A. Petersson and H.R. Simonsen, Improved large-mode-area endlessly single-mode photonic crystal fibers, Opt. Lett. **28** (6) (2003) 393–395.

[39] T.P White, R.C. McPhedran, C.M. de Sterke, L.C. Botten, M.J. Steel, Confinement losses in microstructured optical fibers, Opt. Lett. **26** (21) (2001) 1660–1662.